Synthesis of the SWCNTS/TiO2 Nanostructure and Its Effect on the Thermal, Optical, and Conductivity Properties of the CMC/PEO as Application of Low Energy Density Devices

qana A. alsulami
King Abdulaziz University
A. . Rajeh (a.rajeh88@yahoo.com)
Amran University

Research Article

Keywords: TiO2 nanoparticles, SWCNTs/TiO2 nanohybrid, TEM, thermal properties, AC conductivity

Posted Date: July 1st, 2021

DOI: https://doi.org/10.21203/rs.3.rs-621763/v1

Abstract

The TiO_2 NPs synthesized by sol-gel method and the SWCNTs/TiO_2 nanostructure fabricated by a simple mixing technique. By a solution casting process, pure CMC/PEO and SWCNTs/TiO_2 nanohybrid doped CMC/PEO polymer blend films are prepared. It discussed the influence of polymer blend and MWCNTs/TiO_2 nanohybrid loading on the properties of physical of the polymer blend. The XRD pattern shows that the average crystallite size of the nanoparticles for TiO_2 and SWCNTs/TiO_2 is 20 nm and 15 nm, respectively, and an increase in amorphicity was observed with an increase in doping. The interaction of CMC/PEO chains and SWCNTs/TiO_2 nanohybrid is confirmed by FTIR spectra. The optical absorption spectrum shows that the energy gap reduces with the dopant increase. The miscibility between the CMC and PEO is demonstrated by DSC thermograms. An Enhancement in the thermal stability of the prepared samples with an increase in content of dopant is seen in the TGA analysis. The maximum value of the blend's AC conductivity is 4.77 10^{-5} S/m, and by increasing the loading of SWCNTs/TiO_2 to 4.8 (wt.%) increased to 8.07 10^{-4} S/m. The conduction mechanism changed with SWCNTs/TiO2 loading from the correlated barrier hopping, in the blend, to the large Polaron tunneling. Usage of these nanocomposite films in the semiconductor industry is encouraged by the observed improvements in optical, thermal, and AC conductivity.

1. Introduction

Solid polymer electrolytes (SPEs) are significant materials for electrochemical usings ranging from energy storage systems (fuel cells/supercapacitors/batteries) to photoelectrochemical solar cells, and electrochromic displays[1–3]. Due to its striking characteristics, such as no electrolyte leakage, flexibility, the temperature range of the operating wide of the devices, and long-term protection, the solid state polymer batteries have attracted interest. Hence, polymer electrolytes and their use in lithium ion rechargeable solid state batteries are thus well identified for research and development, as they can easily replace the liquid electrolytes now utilized in state-of-the-art energy storage devices[4]. Researchers' attention has shifted to the mixing of polymers over the past few years, opening up a new wave of potential as an adequate method for improving the structural, conductivity, optical, and thermal properties of electrolyte systems[5,6]. The mixing of polymers together creates more complex sites that increase ion migration, leading to an increase in ionic conductivity[7]. Doping metal oxide, nano-metal oxide, CNTs, etc. can also modulate the ionic conductivity of polymer-based electrolytes[8]. PEO, PVA, PVP are artificial polar polymers used in the development of proton-conducting samples[9,10]. However, natural polar polymers such as cellulose, starch, and chitosan have been utilized to make proton-conducting electrolyte films[11,12]. The structural, thermal, mechanical and electrical properties of these polymers have been significantly reformed when they are complexed with different dopants, such as (inorganic-organic) acids or salts[13]. The most abundant biomass materials in nature is cellulose[14]. The most common and cheapest ionic-type smart cellulose ether is carboxymethyl cellulose (Na-CMC). It is generated under rigidly regulated conditions through the reaction of alkali cellulose with sodium monochloroacetate. It has strong film-forming properties, high mechanical resistance, and a high degree

of transparency[15]. Na-CMC is also a substance that is both biodegradable and non-toxic [16]. These properties and functions make it suitable for utilization in a wide range of applications, such as food packaging[17], production of coatings[18], gas separation properties, wound dressing, drug delivery systems[19], agricultural applications[20], sensing of liquid petroleum gas[21], and as a binder for Li-ion battery anodes[22]. PEO is a semi-crystalline artificial polymer, on the other hand, and has the general molecular structure $(CH_2CH_2O)n$. Due to its water solubility, high crystallinity, low toxicity, and biocompatibility, PEO, as a commercially prominent thermoplastic polymer, has wide application in many fields[23]. Furthermore the flexible C-O-C stretching structure in the backbone of the PEO chain gives excellent durability for the material[24]. Many researchers have been attracted to studying the impact of various dopants on the chemical and physical properties of the CMC. Rozali et al. [25] reported the preparation of SPE based on adipic acid-incorporated with CMC. The effect on the CMC properties by adding the NiCl [26], CNTs, Cs[27], and TiO_2[28] has also been reported. Furthermore, Yadava et al. [29]synthesized a graphene oxide (GO, at 1 wt%)/CMC/alginate composite with 1128 and 40 % enhanced young's modulus and tensile strength, respectively. Zhan et al. [30] Produced a GO/PAM/CMC nanocomposites with enhanced compressive strength (at 1.6 wt%). Another working group indicated that TiO_2 nanoparticles doping of PVA/Cs/$LiClO_4$ composites could be utilized in lithium-ion batteries because it promotes the movement of polymer matrix lithium ions[31]. Single-walled carbon nanotube (SWCNT) is electrical conductors and their incorporation into TiO_2 could increase the mobility of photogenerated electrons. By driving these electrons more efficiently, from TiO_2 to steel, SWCNTs can stop corrosion. By maintaining a low potential, these electrons will therefore slow down the process of oxidation. In addition, the incorporation of SWCNTs can change the TiO_2 super-hydrophilicity[32]. Finally, by decreasing the electron-hole recombination rate, photoactivity and conductivity can be enhanced. Indeed, SWCNTs play a role in the transfer of electrons and allow a reduction in electron-hole pair recombination[33]. In this study, due to their superior mechanical and strong charge storage ability, CMC and PEO were chosen as host polymers. As a strong proton donor to the polymer matrices, SWCNTs/TiO_2 was selected as a dopant and is ideal for the application of low-energy-density devices. CMC/PEO doped with SWCNTs/TiO_2-based solid polymer electrolytes was used in this current system to test optical, thermal, and electrical properties.

2. Experimental Work

2.1 Materials

ACROS, New Jersey and USA purchased the powder of PEO with MW ≈ 40000 g/mol. Sigma-Aldrich sealed Carboxymethyl cellulose with MW ≈ 250,000. Nanothinx, Greece, produced SWCNTs-COOH functionalized (diameter of 6–15 nm, length ≥21 μm, and a purity of 92%) and titanium disopropoxide (Ti $(OPr)_4$, bis (acetylacetonate), isopropanol (Aldrich). In the preparation for polymer blend and nano-composites distilled water was used as a solvent.

2.2. Preparation of pure TiO_2 nanoparticles

A sol-gel method was used to prepare TiO_2 NPs. At 60 °C with constant stirring for one hour, Titanium tetra isopropoxide and (20 mL), ethanol (90 mL) was mingled. Then a drop wise of the deionized water was used until the milky colored precipitate. For a complete removal of organic solvent and filtered, the precipitate was cleaned several times with water. To get the pure TiO_2 nanoparticles, this precipitate was dehydrated in oven air at 110 °C for half hour and then annealed at 400 °C for three hours.

2.3. Preparation of SWCNTs /TiO_2 nanohybrid

To obtain a homogeneous mixture, 20mg SWCNTs and 250 mg as-prepared TiO_2 NPs were typically melted in deionized water and probe sonicator for half-hour. The suspension was then stirred well for 12 hours at 85°C. After the product was filtered, distilled water and ethanol were used to wash it for four times, and dried under vacuum conditions at 75 °C for one day. Eventually, the powders were processed in a furnace at 350°C for 2 hours in a nitrogen environment to produce SWCNTs/TiO_2 nanohybrid.

2.4. Preparation of the CMC/PEO-SWCNTs/TiO_2 nanocomposites

The solution-cast method was used to make (CMC/PEO)–x wt% TiO_2/SWCNTs films using CMC, PEO, and TiO_2/SWCNTs. Weight quantities of 30% PEO and 70% CMC were dissolved in water in separate glass containers for each sample, and then these polymeric solutions were combined under magnetic stirring to get the blend homogeneous solution. The requisite quantity of TiO_2/SWCNTs was first distributed in water for the x wt% concentration (x = 0.4, 1.6, 3.2, and 4.8) with respect to the weight of the CMC/PEO blend. After that, the aqueous dispersed TiO_2/SWCNTs were blended into the aqueous CMC/PEO solution, and magnetic stirring was used to achieve a homogeneous solution of (CMC/PEO)–x wt percent TiO_2/SWCNTs. This solution was poured into a polypropylene dish and dried at room temperature, resulting in a free-standing (CMC–PEO)–x wt% TiO_2/SWCNTs film. Following the same steps as before, PNCs films with various TiO_2/SWCNTs concentrations were made. Prior to measurements, the produced PNCs films were drained in a vacuum oven at 45 °C for 1 day.

2.5. Characterizations techniques

The Nicolet iS10 (USA) was utilized to scan the FT-IR spectra of an SWCNTs/TiO2 doped CMC/PEO blend in the region 500-4100 cm^{-1}. In the Bragg's angle range 5–70° and the wavelength equal 1.5407 Å (Cu-Kα) of DIANO Corporation-USA, XRD patterns of specimens were evaluated at volt equal 30 kV. The investigation of nanoparticles size and dispersion was conducted by the help of the TEM through a JEOL 1200 EX model at operating voltage 120 kV. The optical absorption spectra of the prepared specimens were recorded using a JASCO UV-VIS Spectrometer (Model V-630, Japan) at room temperature(RT) from 190 to 900 nm. Thermogravimetric (TGA) curves were measured utilizing a TGA thermal analyzer (STD-Q600, USA) in the temperature range 30–600 °C at a rate of 10 °C min^{-1} in a N_2 atmosphere. The AC analyses were carried out in a dry N2 atmosphere at RT and various temperatures with a frequency range of 10 Hz to 15 MHz using a (Novocontrol turnkey idea 40 System).

3. Results And Discussion

3. 1. XRD

The XRD diffraction spectroscopic technique was employed to study the structure of the polymer composite films. The XRD patterns of SWCNTs, TiO_2 and MWCNTs/TiO_2 nanocomposites are shown in Figure 1. The two broad XRD peaks are visible in the SWCNTs' XRD pattern, at 26.13 and 43.63, which correspond to the graphic carbon planes of (200) and (101), respectively (JCPDS 75-1621)[34,35]. The typical diffraction peaks can be found at 25.46°, 32.45°, 36.23°, 54.09°, 59.06°, 62.89∘, and 71.32°. The as-prepared sample can be classified as anatase TiO_2 when compared to the standard pattern (JCPDS no. 21-1272). The peaks mentioned above correspond to the crystal planes of (101), (004), (200), (211), (204), and (220)[36]. In the range studied, no characteristic peaks of CNT can be found in the spectra of the SWCNTs/TiO_2 nanocomposite. This is due to the overlap of the intense peaks of the CNT (200) and anatase (101) reflections, as well as the relatively wide mass disparity between CNT and TiO_2[37]. The composite material's main diffraction peaks are sharp and display strong crystallinity. In comparison to pure TiO_2 nanoparticles, the intensity of XRD peaks of SWCNTs/TiO_2 nano-hybrid specimens was decreasing (Fig. 1).This shows that the average size of the crystallite of the nanocomposites is smaller, due to TiO_2 NPS adsorption on the SWCNTs surface, which decreased agglomeration and thus crystallite size[38]. The equation of Debye–Scherrer's $D= k\lambda/(\beta \cos\theta)$ was applied to calculate the average crystallite sizes[39], in which k is a constant =0.9 or 1, β is full width at half the diffraction peak's maximum intensity. The estimated crystallite size of the TiO_2 and SWCNTs/TiO_2 was 20 nm and 15 nm, respectively.

The relatively broad diffraction peak positioned at 2θ = 21.54° was revealed in Figure2 which contained the XRD spectra for pure CMC/PEO, this confirm semi-crystalline nature of CMC/PEO due to interaction between chains of the CMC and PEO by hydrogen bonding[40]. The presence of SWCNTs/TiO2 as nanofiller in the pure CMC/PEO[41] was identified by the existence of the peaks along with increase in intensity with content of SWCNTs/TiO2 and decline in the intensity of the diffraction peaks of characteristic of CMC/PEO. On the basis of the XRD patterns of the prepared samples, Bragg's law $d=n\lambda/(2 \sin\theta)$, where n = 1 is reflection order, θ is angle of Bragg's, λ = 1.5405 Å was conducted to estimate the d-spacing. The equation of Debye–Scherrer's was applied to calculate the average crystallite sizes of the samples. Hermans and Weidinger method $X_c=A_c/A_T\times100$ is used to analyze the crystallanity (Xc). In this method, Ac is area of amorphous haloes and A_T is the total area of peaks (area of crystalline and amorphous peak)[42]. The estimated parameters are shown in Table 1. As shown in the Table, a shift to higher angle and a decline in inter planar separation were referred to the characteristic diffraction peak at 21.54^o in nanocomposites (4.8wt.%). It's possible that this is due to the filler molecules being incorporated into the matrix's interplaner spacing [43]. Furthermore the new crystalline peaks (at 2θ =25.46°, 32.45°, 36.23°, 54.09°) identified in CMC/PEO-SWCNTs/TiO_2nano-composite can be compatible with peaks of the pure SWCNTs/TiO_2. The figure also revealed that the formation of the complexation

between nanoparticles and CMC/PEO composite resulted in a rise in the intensity of the crystalline peaks as the loading of filler particles increased. This result is in perfect harmony with the FTIR analysis.

Table 1: XRD parameters of pure blend and SWCNTs/TiO_2 filled polymer blend.

A concentration of CNT/TiO_2 (wt%) NPs in CMC/PEO	2θ (degree)	d-Spacing (Å)	Average size of crystallite (D)	Inter-crystallite separation R (Å)	Crystallanity(%)
0	21.62	4.10	15.32	5.135	55.32
0.4	21.54	4.12	17.14	5.155	48.67
1.6	21.28	4.17	18.41	5.217	35.95
3.2	21.32	4.16	16.87	5.207	38.49
4.8	21.15	4.19	19.54	5.249	33.98

3.2. TEM

The increased resolution of TEM examination allows for a better understanding of the specific details of nanostructures. Figure3(a,b) illustrates TEM images of TiO_2 NPs synthesized by sol-gel and the CNT–TiO_2 nanocomposites fabricated by a simple mixing technique. TEM images of TiO_2 NPs (Fig. 3a) revealed that during the production stage, most of the particles were spherical and clustered to form bigger aggregates, and nanoparticles size were almost (30-22) nm, somewhat larger than the size determined from XRD analysis [20 nm][44]. The presence of well-spread TiO_2 NPs with an essentially narrow size distribution throughout the tube walls of the CNT–TiO_2 sample can be seen in TEM images of the sample (see Fig. 3b). Also, the figure 2b shows that TiO_2 NPs are well ornamented on the surface of CNTs, resulting in CNT–TiO_2 nanocomposites. This suggests that TiO_2 NPs may bind to the surface of CNTs via van der Waals interactions[45].

3.3. FTIR Spectroscopy Analysis

Using FTIR spectroscopy helped to realize the chemical composition and the possible interactions between CMC/PEO and SWCNTs/TiO_2 nanocomposites. The results of analysis also revealed that specific intramolecular and intermolecular interactions of polymer chains caused the complexation to occur between two polymers, and that hydrogen bonding caused the complexation between the CMC/PEO and SWCNTs/TiO_2. The interaction between all the materials was identified by using the IR absorption bands in spite of their observed changes in the position, shape and intensity. All samples recorded by FTIR spectra in the wavenumber range from 500 to 4000 cm^{-1} were shown in Figure 4a. The selection of the highlighted region was regarded to the most interaction existed between the blend and the dopant. At 1059 cm^{-1}, which attributed by C–O- stretching of pure CMC, the vibrational bands are noticed[46]. Up to the level of CMC/PEO/ (4.8 wt.%) SWCNTs/TiO_2, the decrement of intensity and

increment of the broadness was observed. The analysis also revealed that a slight shift from higher to lower wavenumber of 1059 to 1045 cm^{-1} appeared. The occurrence of such slightly shift was regarded to the existence of oxygen from C–O- interacted with OH or COOH groups from SWCNTs presence in the SWCNTs/TiO_2. In the other side, Mazuki et al suggested that the band at 1323cm^{-1} is assigned to -OH bending[47]. The peaks observed between 2908 and 2845 cm^{-1} were similar and dissimilar C–H_2 bond's osculation. In Fig. 2a, the band at 3331 cm^{-1} relates to O–H stretching is noticed. The hydroxyl band intensity was decreased upon the addition of the Nano-filler. This reflection might refer to the complexation of SWCNTs/TiO_2 with blend. As noted in Figure 4b, the intensity of the peak at this band reduced upon the adding of SWCNTs/TiO_2 NPs and changed into the high wavenumber (1330 cm^{-1}). At 1589 cm^{-1} wavenumber a remarkable band existed, which relates to C=O of COO-. Such a results belongs to CMC/PEO blend[48]. In regards, when the content of the Nano-filler is added to the polymer blend, the peaks begin to decrease. Mejenom et al.[49]stated that due to the creation of intermolecular hydrogen bonding between the C=O of the CMC/PEO with the SWCNTs/TiO_2 surface, the peak shifting might occur. The interaction between OH^+ and Ti^+ in the SWCNTs/TiO_2 can explain this shifting, with ether group in the polymer blend where the lone pair electron of oxygen will attract the Ti molecule to stick to it and then contribute towards the protonation process as shown in scheme1[50].

3. 4. DSC studies

DSC is used to study the thermal response of SWCNTs/TiO_2 doped CMC/PEO polymer nanocomposites and the thermograms of the existing nanocomposites films are displayed in Figure 5. The DSC curves of nanocomposites films mainly give the sample three characteristic temperatures, i.e. the temperature of the transition of the glass(Tg), the temperature of melting, and the temperature of degradation. The transformation takes place in the polymer matrix as the temperatures is increased by the temperature of the glass transition and includes the onset of motion and bond rotation of the thermally induced chain segment. The transition of glass is therefore an essential parameter for predicting the polymer's thermal properties[51]. As the midpoint of the region of rising heat flow in all films, the glass transition temperature is measured. Pure CMC/PEO blend has glass transition at 58.67 ° C and by promoting chain mobility; it reduces slightly with the adding of nanofiller, so that ionic conductivity increases with ion motion[52,53]. The CMC/PEO/(4.8 wt.%) SWCNTs/TiO_2 film shows the low Tg, which induces the higher segmental motion of polymer chain. The ions can easily pass across the polymer matrice in this system, i.e., there is high ionic mobility. This will help boost the transport of ions and the complex system of CMC/PEO/(4.8 wt.%) SWCNTs/TiO_2 NPs displays elevated electrical conductivity. In addition, the observed change in T_g values of the prepared films in DSC thermograms suggests that the blend-SWCNTs/TiO_2 NPs interaction confirms the complexation [54]. The presence of one glass transition temperature in the CMC/PEO blend confirms the miscibility between CMC and PEO[55]. As the doping of SWCNTs/TiO_2 (251.79-267.56 °C) increases, the melting temperature of the polymer nanocomposite rises due to the obstruction of the polymer chain's mobility and rotation. The melting point is boosted by the rise in the energy barrier. At higher temperatures, the thermal stability of polymer blending increases with

doping content. The increase in driving force makes the degradation temperature to rise from 307 to 293 ° C due to the interaction of SWCNTs/TiO_2 with the CMC/PEO blend[31].

3. 5. Thermogravimetric (TGA)

Thermal stability of PSEs is an important parameter in the manufacture of electrochemical devices that are supported and endurable. A particular technique that can be used to examine the thermal stability of prepared films is thermogravimetric analysis (TGA). Weight loss after heating the samples over the temperature range of 15 to 700 ^{o}C can be used to reflect the thermal stability of the films. TGA thermograms of pure blend and various contents of doped CMC/PEO films of MWCNTs/TiO_2 NPs are shown in Figure 6. Three different stages of deterioration are revealed by examination of TGA curves. The first stage was observed at 35-130 ^{o}C, and the water was completely evaporated or dehydrated in this area, according to Ahmad et al. [56]. In polymer systems, the moisture content determines the percentage of initial weight loss. Liu et al.[57] reported a similar finding, where the first stage corresponds to the decrease of film moisture through the process of dehydration and evaporation that leads to the initial loss of weight. The second stage of weight loss can be due to the method of decomposition of polymer systems and the maximum decomposition temperature has reached 355 ^{o}C. In the CMC-PEO backbone, the CO_2 from the carboxylate groups (COO-) has decomposed and thus contributes to a sudden decrease in weight loss[58] Meanwhile, at a temperature range of 280-355 ^{o}C, the decomposition of bond scission in the backbone of the blend is thought to have occurred[59]. This reveals that the temperature of decomposition for the entire samples is beginning to rise with the addition of nanofiller in the current system. This could be due to the entire content creation of homogeneous polymer electrolytes, allowing CMC-PEO to obtain any charge of ionic[60]. Based on this process, it is clear that when MWCNTs/TiO_2 NPs are introduced into the system, CMC-PEO would provide more ion hopping sites and thus lead to an increase in temperature of decomposition. Su et al.[61] stated that the Millard reaction and crosslinking between the two polymers and nanomaterials lead to the improvement of thermal stability by generating more free volume space when two different polymers have been blended with nanomaterials.

3. 6. UV-Vis. analysis

The UV–Vis spectra of CMC/PEO blend and Nano-composites films were shown in Figure 7. Owing to the presence of C=C and/or C=O mainly in the tail–head of the blend film, the absorption band at 198 nm in polymer blend was ascribed to n-p* transitions and around 215 nm was attributed to p - p*. It can be noted that various SWCNTs/TiO_2 were treated by blend. Note that blend doped various SWCNTs/TiO_2 nanoparticles contents the absorption bands and band edges of the SWCNTs/TiO_2 doped polymer blend have shifted towards higher wavelengths, with varying absorption intensities[62].These band shifts confirm the formation of inter/intramolecular hydrogen bonds, primarily between SWCNTs/TiO_2 ions and adjacent functional groups of the polymer blend that are consistent with FTIR results. The change in the energy band-gap in the doped polymer blend reflects the difference in crystallinity within the polymeric matrices which results in a shift in the absorption edge that are consistent with XRD results[53].

3. 6. 1. Measurement of optical energy band gap

The relationship between the absorption coefficient (a) and Eg, is well known to obey the classical Tauc's expression. The optical energy band gap is calculated using the observed UV–Vis spectra by translating the spectra into Tauc's plots. We use Mott and Devis' frequency-dependent a to convert the absorption spectrum into Tauc's plot[53].

$$\alpha(v) = \beta(hv-Eg)^n / hv \qquad (1)$$

where n is an empirical index equal to 0.5 or 2 for direct or indirect allowed transition in the quantum mechanical sense and β is a constant. Figure 8(a, b) shows the calculated Eg for all of the samples as well as their variations. The bandgap reduces as dopant concentration rises, as shown in Figure 5(a, b). The presence and change of the optical energy gap Eg can be explained by assuming that cross-linking occurs within the amorphous phase of the polymer blend, reducing the ordering degree in these parts[39]. As observed in FTIR studies, the ions in SWCNTs/TiO_2 interact with functional groups of polymer blend and create a complex through intramolecular and intermolecular hydrogen bonding.

3. 7. AC conductivity

The AC impedance analysis can be used to understand the electro-activity of polymeric materials. The AC conductivity of the CMC/PEO blend and MWCNTs/TiO_2 doped CMC/PEO nanocomposites is shown in Figure 9a at different frequencies varying from 100 to 10^6 Hz. It can be observed that, because the trap charges in the polymer matrices are not in equilibrium, the AC conductivity is observed to be weakly frequency (*f*) dependent at the low frequency region and the ions can reside relatively for a long time, and thus there is more accumulation of charge at the electrode/electrolyte interface, which delays ion mobility and consequent decrease in conductivity[39]. The conductivity revealed an exponential increase in the high frequency region with *f* of electrical field applied suggesting charge carrier hopping[50]. The embedded blend of SWCNTs/TiO_2 has the highest conductivity than that of the pure blend. In the CMC/PEO blend, the uniform distribution of nanofiller increases the normal orientation of the nanocomposites, leading to higher AC conductivity. Up to 3.2 wt.% of SWCNTs/TiO_2 loading is observed of the optimum conductivity of the nanocomposite and after that the conductivity is observed to be reduced, these findings comply with previous study[63]. This means that the grain boundaries are enhances by the interfacial interaction between SWCNTs/TiO_2 and the CMC/PEO blend, and this is higher at 3.2 wt.% dopant. The uneven distribution of SWCNTs/TiO_2 in the polymer matrices contributes to the creation of aggregates or clusters in the nanocomposite, which restricts the mobility of charge carriers through the polymer matrice and thus reduces the ac conductivity at a higher nanofiller loading (4.8 wt.% of SWCNTs/TiO_2)[64]. The improvement in ionic conductivity with the increasing content of SWCNTs/TiO_2 nanoparticles may be due to the interaction of the nanoparticles with both the anion and cation. The ion-pairing is obstructed by this and the free charge carriers are increased. The SWCNTs/TiO_2 nanoparticles filler enhances the ionic conductivity of nanocomposite by impeding the reorganization of the crystalline phase of CMC/PEO chains, according to the Lewis acid-base model[65]. Compared to that

of the pure blend, the size of the filler is very small; the filler is able to penetrate into the polymer matrice and facilitate interaction between ions, plasticizer, and molecules of the polymeric matrix chains. The cohesive force between the chains of polymer is thus decreased and gives a more flexible segmental chain movement as well as MWCNTs/TiO_2ions conducting pathway at the filler surface[66]. The ionic conductivity mechanism of MWCNTs/TiO_2 (3.2wt.%) doped CMC/PEO nanocomposites was investigated at temperatures ranging from 300 to 398 K as shown in figure 9b. As the temperature increases, it is obvious that the charge carriers are activated thermally, and the free volume increases. Therefore, via the coordinated ether oxygen sites, more vacant sites are produced for the ions hopping , which in turn increases conductivity[67]. As shown in Figure 10, the s-value for SWCNTs/TiO_2 (3.2wt. %) doped CMC/PEO nanocomposites, examined from the slope of the linear parts of the plots in Figure 8b, and was plotted with temperature. As can be pointed out, $0 < s < 1$. The value of s reduces with rising temperature for the SWCNTs/TiO_2 (3.2wt. %) doped CMC/PEO. It reduces at first, however, for the nanocomposite sample, and then increases with temperature. The correlated barrier hopping (CBH)[68] and the large Polaron tunneling (LPT) models are the best-suited mechanism for electrical conduction in the sample on the basis of these results[69]. The charge carrier hops between the sites over the potential barrier dividing them in the CBH model.

3. 8. Dielectric constant

Using dielectric analysis, the ion dynamics in the polymeric matrices were investigated. The variance of dielectric permittivity in the real ε' and imaginary ε" of prepared samples at RT is presented in Figure 11(a, b). The ε' in the material depends on the existence of the ions and disorder[70]. The charges polarization at near of the electrodes will lead to high of the ε' at low frequencies. This polarization of electrode is followed the non-Debye nature of the SPEs[68]. At low frequency region, the jump of ions along the applied field in the energy barrier make the dielectric constant is high. There is no hopping of charge carriers in the high-frequency region and oscillation is only accomplished without reaching the surface of electrode. The ε' is therefore constant for all films in the high-frequency region[6]. The dielectric constant value increases up to 3.2 wt.% of SWCNTs/TiO_2 concentration and then decrease.

As shown in Figure12, the Cole-Cole diagram (Argand plots) of the prepared films is plotted to describe the essence of the relaxation mechanism at room temperature. It is obvious that the patterns are distinguished by two semicircles for all films whose centers do not end on the actual part of the axis of the electric modulus (M'). This behavior suggests that the relaxation mechanisms of the studied samples are of the nonDebye model[71]. The semi-circuit radius of the SWCNTs/TiO_2 (3.2 wt.%)/CMC/PEO sample is obviously small compared to CMC/PEO blend and the other samples that confirm the improvement of ionic conductivity[72].

4. Conclusion

A simple solution casting method has been successfully used for preparing the pure blend CMC/PEO and those loaded with SWCNTs/TiO_2 nanocomposites films. To investigate their structural, morphological,

optical, thermal, electrical, and dielectric characteristics, the films were characterized. The TiO_2 and SWCNTs/TiO_2 nanohybrid have average crystallite size of 20 nm and 15 nm respectively. The XRD study reveals that inorganic filler addition decreases the crystallinity degree thus improving ionic conductivity. FTIR revealed the change in the band position of the nanocomposites at 3400 cm^{-1}, 1735 cm^{-1}, and 1607 cm^{-1}, and also verified the active formation of the nanocomposites (CMC/PEO-SWCNTs/TiO_2). The UV-Vis analyses revealed that with the addition of SWCNTs/TiO_2 nanohybrid, the optical band gap (direct and indirect) reduced and the best band gap was found to be 4.23 eV, revealing that band gap values change to towards longer wavelengths due to interband transitions. The presence of a single Tg in the DSC thermograms of the CMC/PEO blend proved the miscibility between the CMC and PEO. Compared to the pure blend, the electrical properties of the nanocomposites revealed improvement in conductivity and dielectric, and higher the conductivity and dielectric were found at CMC/PEO-SWCNTs/TiO_2 (3.2 wt.%) sample due to the increment in amorphicity. These findings are much enhanced than that of the pure blend. Furthermore, it was noted from the measurements that were used in this study that confirm that CMC/PEO composite film with SWCNTs/TiO_2 (3.2 wt.%) has much better optical, thermal, conductivity, and dielectric properties than pure blending. Based on these findings, it is believed that CMC/PEO-based SPEs doped with SWCNTs/TiO_2 may provide new insight into their potential application in energy storage systems.

Declarations

Acknowledgement

This project was funded by the Deanship of Scientific Research (DSR) at King Abdulaziz University, Jeddah, under grant no. (G: 145-247-1442). The authors, therefore, acknowledge with thanks DSR for technical and financial support.

References

1. Abutalib MM, Rajeh A (2020) Influence of MWCNTs/Li-doped TiO2 nanoparticles on the structural, thermal, electrical and mechanical properties of poly (ethylene oxide)/poly (methylmethacrylate) composite. J Organomet Chem 918:121309
2. Morsi MA, El-Khodary SA, Rajeh A (2018) Enhancement of the optical, thermal and electrical properties of PEO/PAM:Li polymer electrolyte films doped with Ag nanoparticles. Phys B Condens Matter 539:88–96
3. Abutalib MM, Rajeh A (2020) Preparation and characterization of polyaniline/sodium alginate-doped TiO2 nanoparticles with promising mechanical and electrical properties and antimicrobial activity for food packaging applications. J Mater Sci Mater Electron 31:9430–9442
4. Appetecchi GB, Croce F, Hassoun J, Scrosati B, Salomon M, Cassel F (2003) Hot-pressed, dry, composite, PEO-based electrolyte membranes: I. Ionic conductivity characterization. Journal of

power sources 114:105–112

5. Rani MSA, Mohamed NS, Isa MIN (2015) Investigation of the ionic conduction mechanism in carboxymethyl cellulose/chitosan biopolymer blend electrolyte impregnated with ammonium nitrate. Int J Polym Anal Charact 20(6):491–503
6. Rajeh A, Morsi MA, Elashmawi IS, Enhancement of spectroscopic, thermal, electrical and morphological properties of polyethylene oxide/carboxymethyl cellulose blends: Combined FT-IR/DFT, Vacuum. 159 (2019) 430–440
7. Hezma AM, Elashmawi IS, Rajeh A, Kamal M (2016) Change Spectroscopic, thermal and mechanical studies of PU/PVC blends. Phys B Condens Matter 495:4–10. https://doi.org/10.1016/J.PHYSB.2016.04.043
8. Patla SK, Mukhopadhyay M, Ray R (2019) Ion specificity towards structureproperty correlation of poly (ethylene oxide) [PEO]-NH4I and PEO-KBr composite solid polymer electrolyte. Ionics 25:627–639
9. Kumar M, Sekhon SS (2002) Ionic conductance behaviour of plasticized polymer electrolytes containing different plasticizers. Ionics 8:223–233
10. Kumar M, Sekhon SS (2002) Ionic conductance behaviour of plasticized polymer electrolytes containing different plasticizers. Ionics 8:223–233
11. Buraidah MH, Teo LP, Majid SR, Arof AK (2009) Ionic conductivity by correlated barrier hopping in NH4I doped chitosan solid electrolyte. Phys B Condens Matter 404:1373–1379
12. Pawlicka A, Dragunski DC, Guimaraes KV, Avellaneda CO (2004) Electrochromic devices with solid electrolytes based on natural polymers. Mol Cryst Liq Cryst 416:105–112
13. Prajapati GK, Roshan R, Gupta PN (2010) Effect of plasticizer on ionic transport and dielectric properties of PVA–H3PO4 proton conducting polymeric electrolytes. J Phys Chem Solids 71:1717–1723
14. Chan CH, Joy J, Maria HJ, Thomas S (2013) Natural rubber-based composites and nanocomposites: state of the art, new challenges and opportunities. Natural Rubber Materials 2:1–33
15. Samsudin AS, Isa MIN (2012) Structural and electrical properties of carboxy methylcellulose-dodecyltrimethyl ammonium bromide-based biopolymer electrolytes system. Int J Polym Mater 61:30–40
16. Mohammed FA (2001) Topical permeation characteristics of diclofenac sodium from NaCMC gels in comparison with conventional gel formulations. Drug Dev Ind Pharm 27:1083–1097
17. Roy N et al (2012) Biodegradation of PVP–CMC hydrogel film: A useful food packaging material. Carbohydrate polymers 89:346–353
18. Tiitu M, Laine J, Serimaa R, Ikkala O (2006) Ionically self-assembled carboxymethyl cellulose/surfactant complexes for antistatic paper coatings. J Colloid Interface Sci 301:92–97
19. Sandeep C, Harikumar SL (2012) Kanupriya." Hydrogels: a smart drug delivery system. IJRPC 2:603–614

20. Raafat AI, Eid M, Magda B, El-Arnaouty (2012) Radiation synthesis of superabsorbent CMC based hydrogels for agriculture applications. Nucl Instrum Methods Phys Res Sect B 283:71–76
21. Ravikiran YT et al (2014) Liquid petroleum gas sensing performance of polyaniline-carboxymethyl cellulose composite at room temperature. Curr Appl Phys 14:960–964
22. Magasinski A et al (2010) Toward efficient binders for Li-ion battery Si-based anodes: polyacrylic acid. ACS Appl Mater Interfaces 2:3004–3010
23. Lee J, Bhattacharyya D, Easteal AJ, Metson JB (2008) Properties of nano-ZnO/poly (vinyl alcohol)/poly (ethylene oxide) composite thin films. Curr Appl Phys 8:42–47
24. Abd El-Kader FH et al (2005) Relaxation phenomenon of poly (vinyl alcohol)/sodium carboxy methyl cellulose blend by thermally stimulated depolarization currents and thermal sample technique. J Appl Polym Sci 95:1342–1353
25. Rozali MLH, Isa MIN (2014) Electrical behaviour of carboxy methyl cellulose doped adipic acid solid biopolymer electrolyte. International Journal of Material Science 4:59
26. El-Bahy ZM, Khaled H, Mahmoud (2012) Dielectric characterization and catalytic activity studies of nickel chloride doped carboxymethyl cellulose films. Spectrochim Acta Part A Mol Biomol Spectrosc 92:105–112
27. Hafiza MN, Isa MIN (2014) Ionic conductivity and conduction mechanism studies of CMC/chitosan biopolymer blend electrolytes. Research Journal of Recent Sciences 2277:2502
28. Abdel-Galil A et al (2014) Influence of nanostructured TiO2 additives on some physical characteristics of carboxymethyl cellulose (CMC). Journal of Radiation Research Applied Sciences 7:36–43
29. Yadav M, Rhee KY, Park SJ (2014) Synthesis and characterization of graphene oxide/carboxymethylcellulose/alginate composite blend films. Carbohydrate polymers 110:18–25
30. Zhang H, Zhai D, He Y (2014) Graphene oxide/polyacrylamide/carboxymethyl cellulose sodium nanocomposite hydrogel with enhanced mechanical strength: preparation, characterization and the swelling behavior. RSC Adv 4:44600–44609
31. Zhu J-M, Zare Y, Kyong Yop R (2018) Analysis of the roles of interphase, waviness and agglomeration of CNT in the electrical conductivity and tensile modulus of polymer/CNT nanocomposites by theoretical approaches. Colloids Surf A 539:29–36
32. Hou X, Yao K, Wang X, Li D, Liao B (2014) Enhanced superhydrophilicity of N + implanted multiwalled carbonnanotubes-TiO2 composite thin films. Vacuum 100:74–77
33. Réti B, Mogyorósi K, Dombi A, Hernádi K (2014) Substrate dependent photocatalytic performance of TiO2/MWCNT photocatalysts. Appl Catal A 469:153–158
34. Badawi A et al. “Cd0. 9Co0. 1S nanostructures concentration study on the structural and optical properties of SWCNTs/PVA blend.” Chemical Physics Letters (2021) 138701
35. Cheng L, Wang Q, Ding J (2021) Synthesis of Co/CoO@ RGO composite for enhanced electromagnetic microwave absorption performance. Appl Phys A 127:1–12

36. Huo J et al (2014) In situ surface hydrogenation synthesis of Ti 3 + self-doped TiO 2 with enhanced visible light photoactivity. Nanoscale 6:9078–9084
37. Chen Z et al (2016) Novel one-step synthesis of wool-ball-like Ni-carbon nanotubes composite cathodes with favorable electrocatalytic activity for hydrogen evolution reaction in alkaline solution. J Power Sources 324:86–96
38. Alsulami QA (2021) Structural, dielectric, and magnetic studies based on MWCNTs/NiFe 2 O 4/ZnO nanoparticles dispersed in polymer PVA/PEO for electromagnetic applications. J Mater Sci: Mater Electron 32:2906–2924
39. Abutalib MM, Rajeh A (2020) Influence of ZnO/Ag nanoparticles doping on the structural, thermal, optical and electrical properties of PAM/PEO composite. Phys B Condens Matter 578:411796. https://doi.org/10.1016/J.PHYSB.2019.411796
40. Chandrakala HN, Ramaraj B (2014) Optical properties and structural characteristics of zinc oxidecerium oxide doped polyvinyl alcohol films. J Alloys Compd 586:333–342
41. Chatterjee K et al (2011) Bismuth nitrate doped polyaniline–Characterization and properties for thermoelectric application. Synthetic metals 161:275–279
42. Hezma AM, Elashmawi IS, Rajeh A, Kamal M (2016) Change Spectroscopic, thermal and mechanical studies of PU/PVC blends. Phys B Condens Matter 495:4–10. https://doi.org/10.1016/j.physb.2016.04.043
43. Chen R et al (2005) Controlled synthesis of high crystalline bismuth sulfide nanorods: using bismuth citrate as a precursor. J Mater Chem 15:4540–4545
44. Ravishankar TN, Nagaraju G, Dupont J (2016) Photocatalytic activity of Li-doped TiO2 nanoparticles: synthesis via ionic liquid-assisted hydrothermal route. Mater Res Bull 78:103–111
45. Ashkarran AA et al (2015) TiO2 nanoparticles immobilized on carbon nanotubes for enhanced visible-light photo-induced activity. Journal of Materials Research Technology 4:126–132., (n.d.)
46. Kotresh S, Ravikiran YT, Prakash HGR, Ramana CHVV, Vijayakumari SC, Thomas S (2016) Humidity sensing performance of spin coated polyaniline–carboxymethyl cellulose composite at room temperature. Cellulose 23:3177–3186, (n.d.)
47. Mazuki NF, Fuzlin AF, Saadiah MA, Samsudin AS (2019) An investigation on the abnormal trend of the conductivity properties of CMC/PVA-doped NH4Cl-based solid biopolymer electrolyte system. Ionics 25:2657–2667
48. Mazuki NF et al (2020) Studies on ionics conduction properties of modification CMC-PVA based polymer blend electrolytes via impedance approach. Polym Testing 81:106234
49. Mejenom AA, Hafiza MN, Mohamad Isa MIN (2018) X-Ray diffraction and infrared spectroscopic analysis of solid biopolymer electrolytes based on dual blend carboxymethyl cellulose-chitosan doped with ammonium bromide. ASM Sci J 11:37–46
50. Ahmad NH, Isa MIN, Structural and ionic conductivity STudies of CMC based polymerelectrolyte doped with NH4Cl, Adv. Mater. Res., Trans Tech. Publ. (2015) 247–252

51. Khan U et al (2007) The effect of solvent choice on the mechanical properties of carbon nanotube–polymer composites. Composites Science Technology 67:3158–3167
52. El-Hadi A et al (2002) Correlation between degree of crystallinity, morphology, glass temperature, mechanical properties and biodegradation of poly (3-hydroxyalkanoate) PHAs and their blends. Polym Test 21:665–674
53. Bhajantri RF et al (2006) Microstructural studies on BaCl2 doped poly (vinyl alcohol). Polymer 47:3591–3598
54. Bhavani S et al (2017) Studies on structural, electrical and dielectric properties of nickel ion conducting polyvinyl alcohol based polymer electrolyte films. J Mater Sci: Mater Electron 28:13344–13349
55. Mansour LM, BAKHSH, MAHMOUD TAJ, and MASOUD MOKHTARI. “Synthesis and swelling characterization of cross-linked PVP/PVA hydrogels.” (2005) 1022–1030
56. Ahmad NH, Isa MIN (2016) Characterization of un-plasticized and propylene carbonate plasticized carboxymethyl cellulose doped ammonium chloride solid biopolymer electrolytes. Carbohydr Polym 137:426–432
57. Liu X, Yu L, Liu H, Chen L, Li L (2008) In situ thermal decomposition of starch with constant moisture in a sealed system. Polym Degrad Stab 93:260–262
58. Ma X, Chang PR, Yu J (2008) Properties of biodegradable thermoplastic pea starch/ carboxymethyl cellulose and pea starch/microcrystalline cellulose composites. Carbohydr Polym 72:369–375
59. Saroj AL, Singh RK (2012) Thermal, dielectric and conductivity studies on PVA/Ionic liquid [EMIM][EtSO4] based polymer electrolytes. J Phys Chem Solids 73:162–168
60. Rajendran S et al (2012) Transport, structural and thermal studies on nanocomposite polymer blend electrolytes for Li-ion battery applications. Curr Appl Phys 12:789–793
61. Su J-F, Huang Z, Yuan X-Y, Wang X-Y, Li M (2010) Structure and properties of carboxymethyl cellulose/soy protein isolate blend edible films crosslinked by Maillard reactions. Carbohydr Polym 79:145–153
62. Rajeh A, Ragab HM, Abutalib MM (2020) Co doped ZnO reinforced PEMA/PMMA composite: Structural, thermal, dielectric and electrical properties for electrochemical applications. J Mol Struct 1217:128447
63. Kaur B, Tanwar R, Uttam Kumar M (2020) Effect of Nanoparticles Concentration on Thermal, Magnetic and Electrical Properties of Ni0. 5Zn0. 5Fe2O4 based Polyaniline Nanocomposites by In-Situ Polymerisation. Colloids Surf A 599:124798
64. Sankar S et al (2020) Characterization, conductivity studies, dielectric properties, and gas sensing performance of in situ polymerized polyindole/copper alumina nanocomposites. J Appl Polym Sci 137:49145
65. Croce F et al (2001) Role of the ceramic fillers in enhancing the transport properties of composite polymer electrolytes. Electrochim Acta 46:2457–2461

66. Uma T, Mahalingam T, Stimming U (2004) Conductivity and thermal studies of solid polymer electrolytes prepared by blending polyvinylchloride, polymethylmethacrylate and lithium sulfate. Mater Chem Phys 85:131–136
67. Singh NK, Mohan L, Verma, Minakshi M (2015) PEO nanocomposite polymer electrolyte for solid state symmetric capacitors. Bull Mater Sci 38:1577–1588
68. Abdelrazek EM, Elashmawi IS, Hezma AM, Rajeh A, Kamal M (2016) Effect of an encapsulate carbon nanotubes (CNTs) on structural and electrical properties of PU/PVC nanocomposites. Phys B Condens Matter 502:48–55. https://doi.org/10.1016/j.physb.2016.08.040
69. Prajapati GK, Gupta PN (2009) Conduction mechanism in un-irradiated and γ-irradiated PVA–H3PO4 polymer electrolytes. Nucl Instrum Methods Phys Res Sect B 267:3328–3332
70. Popa S et al (2017) Solid polymer electrolytes based on phosphorus containing polymers for lithium polymer batteries. Eur Polymer J 94:286–298
71. Thakur S et al (2016) Impedance and modulus spectroscopy characterization of Tb modified Bi0. 8A0. 1Pb0. 1Fe0. 9Ti0. 1O3 ceramics. Materials Research 19:1–8
72. Alghunaim N, Suliman (2018) Structural, thermal, dielectric spectroscopic and AC impedance properties of SiC nanoparticles doped PVK/PVC blend. Results in Physics 9:1136–1140

Figures

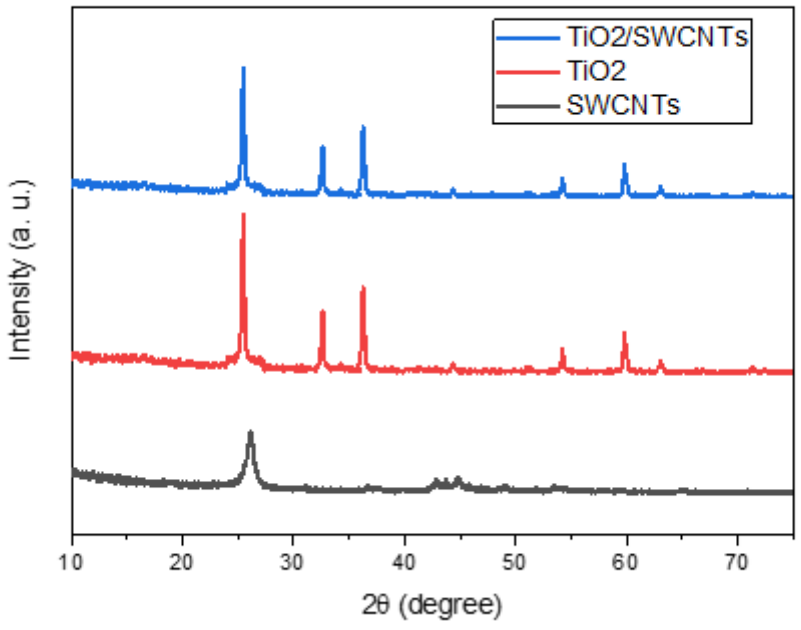

Figure 1

XRD for SWCNTs NPs, TiO2 NPs, and SWCNTS/TiO2 nanohybrid.

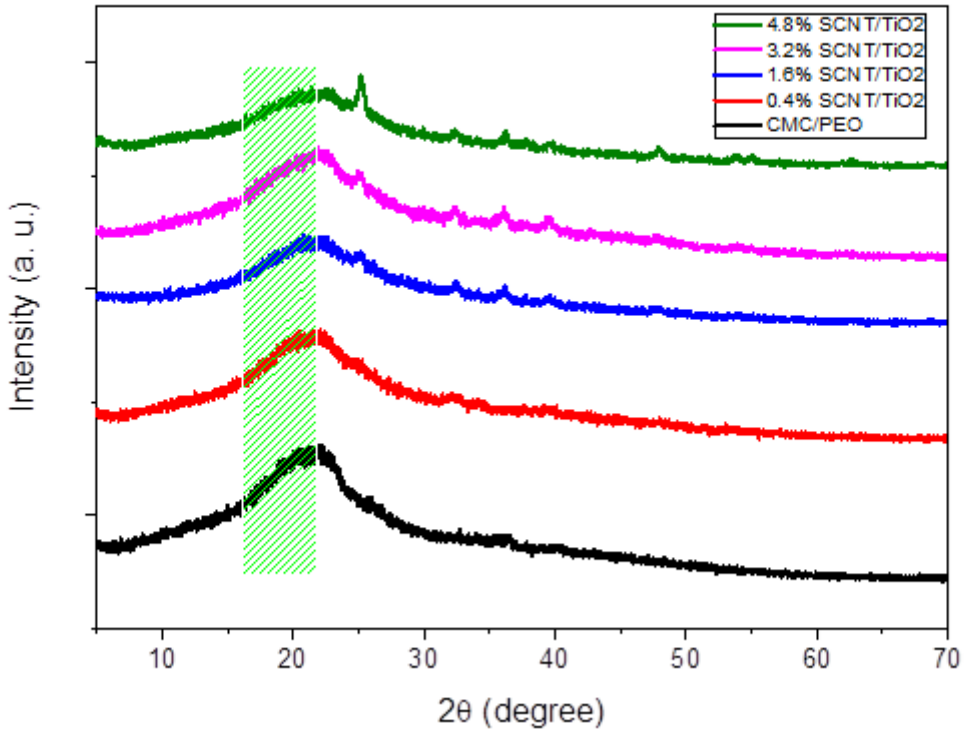

Figure 2

XRD patterns for CMC/PEO and CMC/PEO-(SCNTs/TiO2 wt.%) nanocomposite samples.

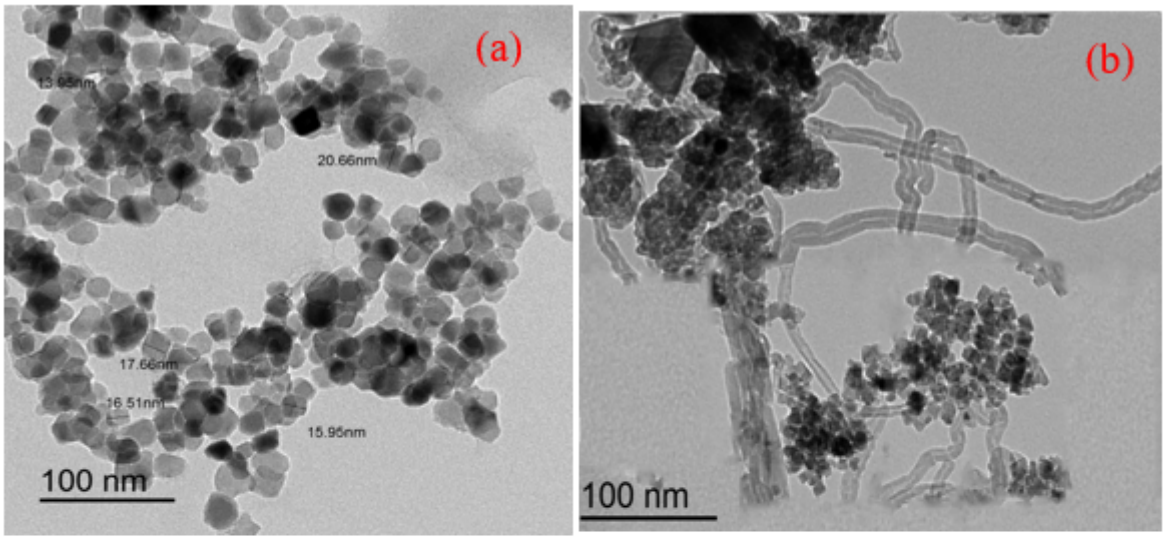

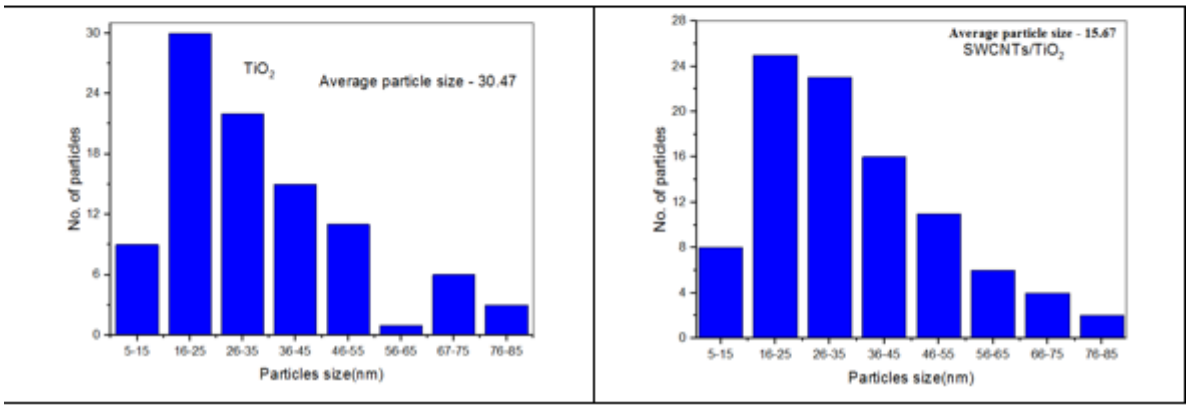

Figure 3

TEM images and Histograms of particle size distribution of (a) TiO2 NPs, (b) SW CNT/TiO2 nanohybrid.

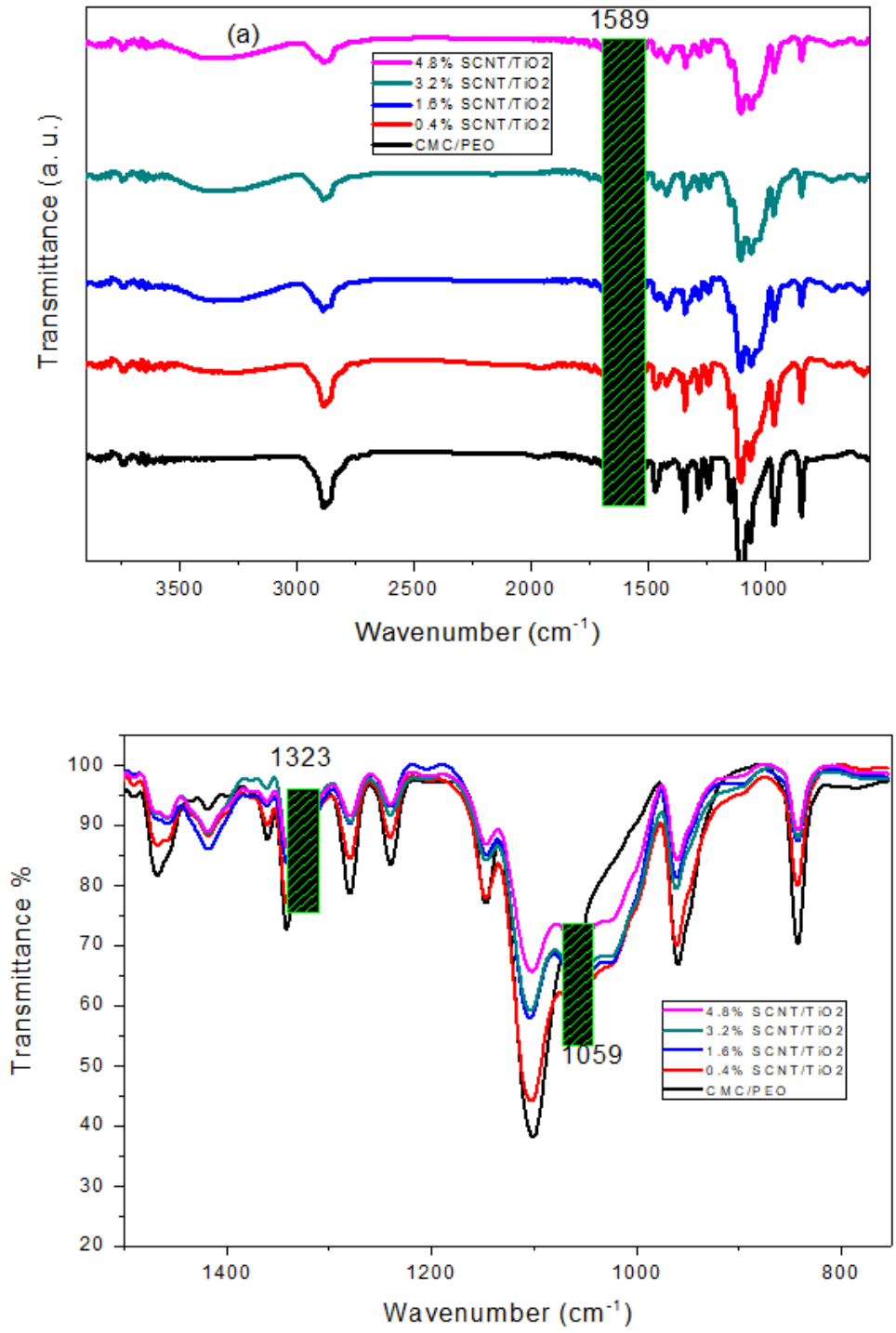

Figure 4

FT-IR spectra for CMC/PEO and CMC/PEO-(SCNTs/TiO2 wt.%) nanocomposite samples (a) 4000-500 cm-1 (b) 1500-750 cm-1.

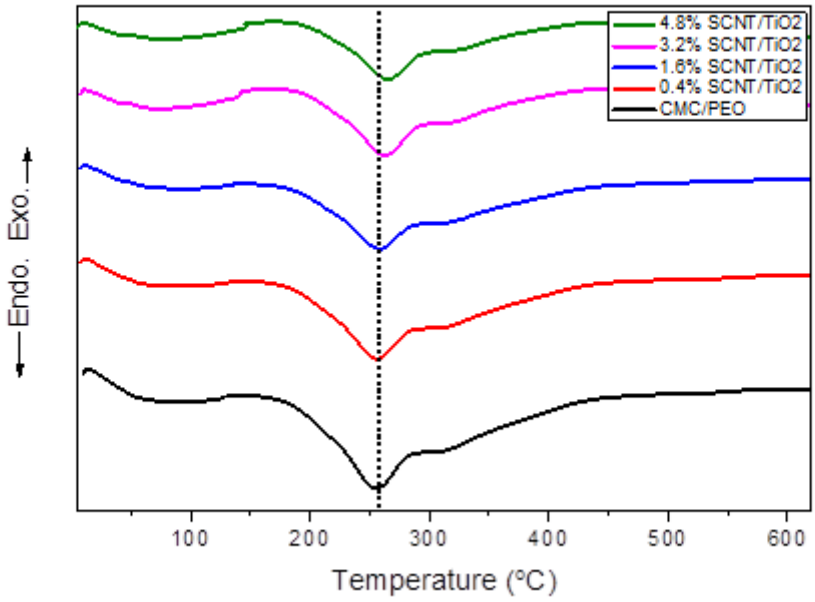

Figure 5

DSC thermograms for CMC/PEO and CMC/PEO-(SCNTs/TiO2 wt.%) nanocomposites samples.

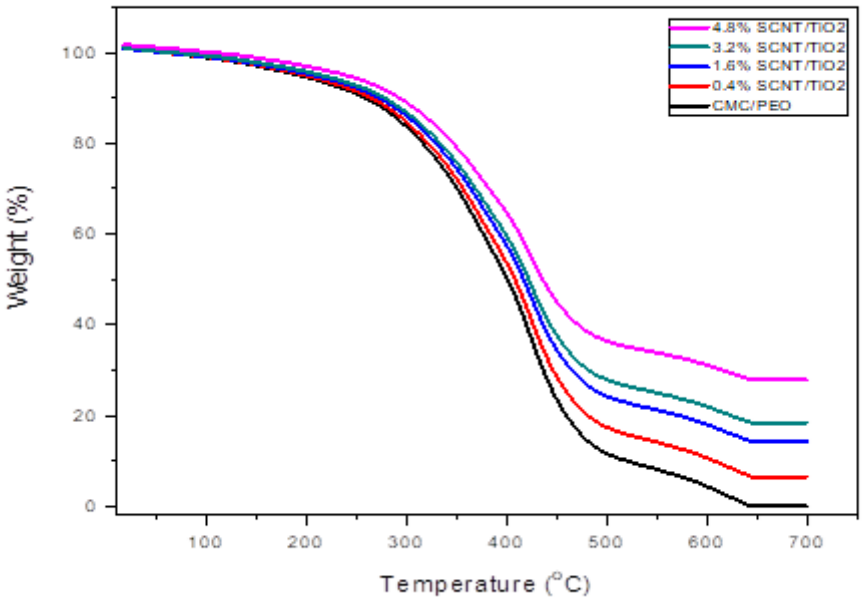

Figure 6

TGA curves of CMC/PEO and CMC/PEO-(SCNTs/TiO2 wt.%) nanocomposite samples.

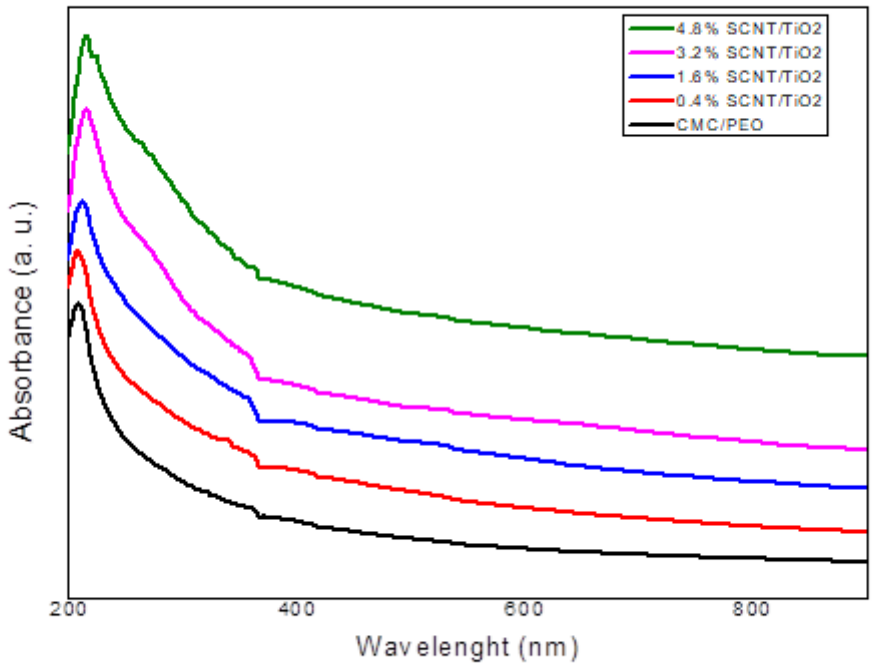

Figure 7

Absorbance curves for CMC/PEO and CMC/PEO-(SCNTs/TiO2 wt.%) nanocomposite samples

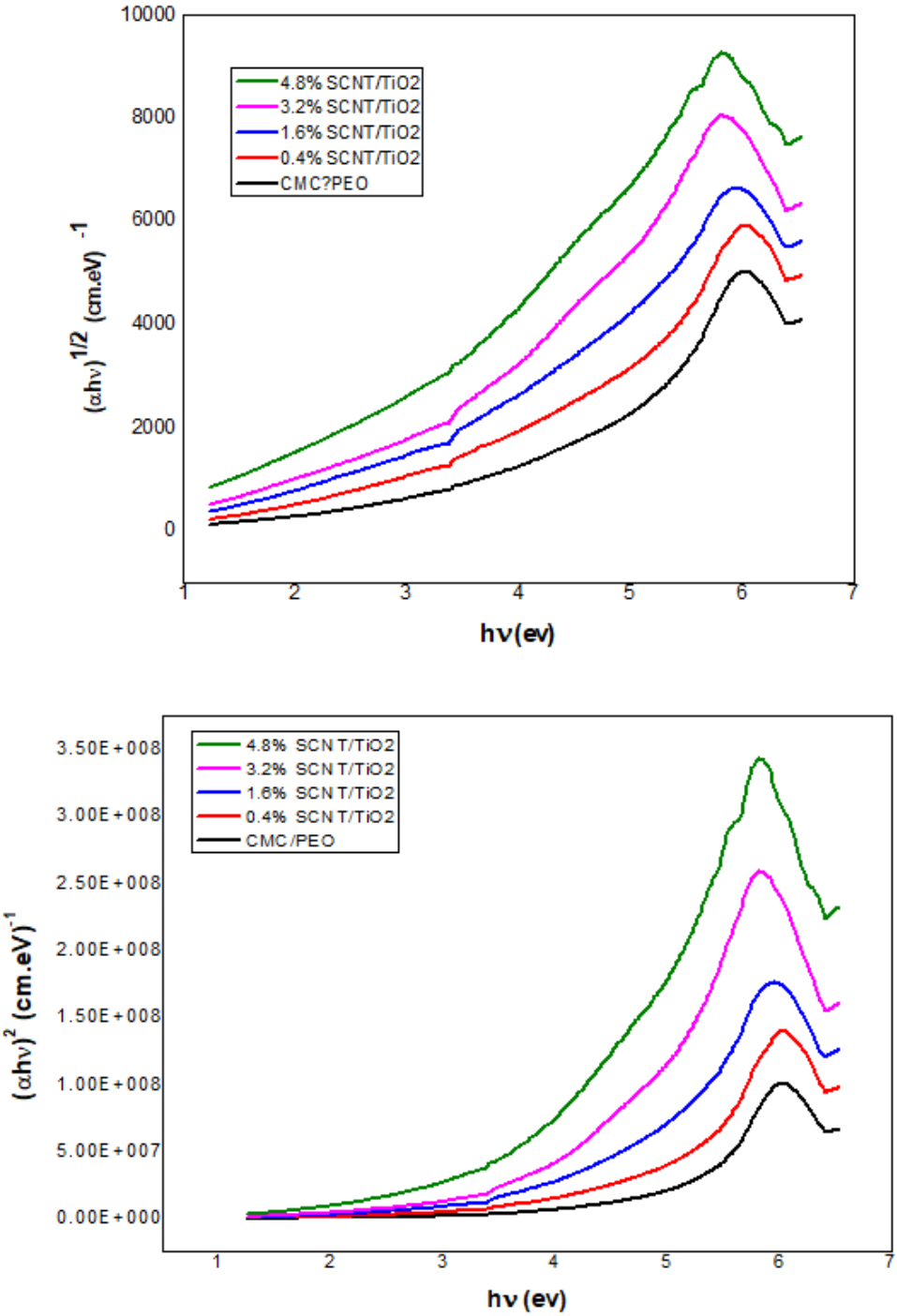

Figure 8

Variations of a (αhυ)1/2 and b (αhυ)2 with hυ of CMC/PEO and CMC/PEO-(SCNTs/TiO2 wt.%) nanocomposites samples.

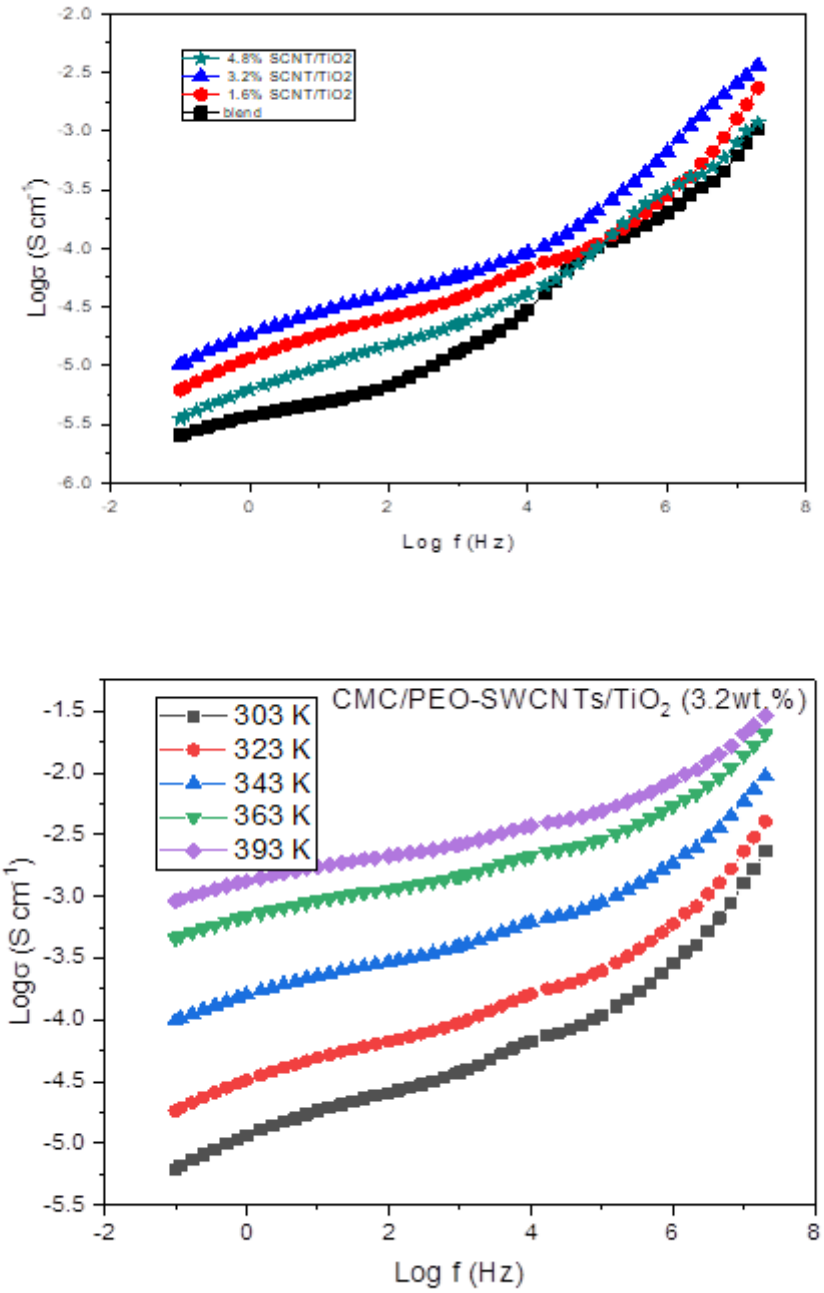

Figure 9

Frequency dependent ac conductivity of CMC/PEO and CMC/PEO-(SCNTs/TiO2 wt.%) nanocomposite samples (a) at room temperature (b) at different temperature.

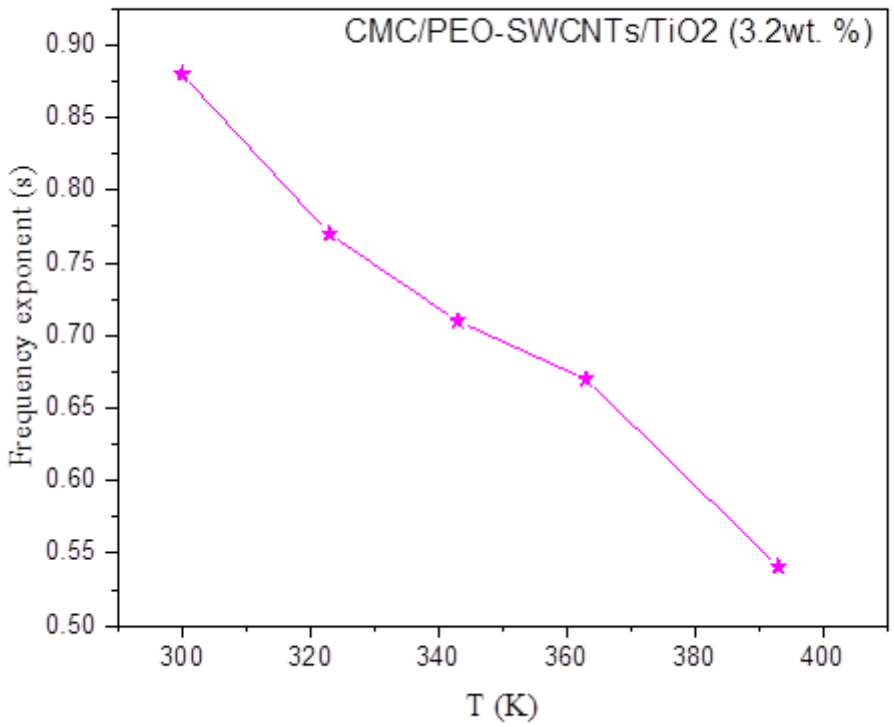

Figure 10

Relation of S with Temperature for SWCNTs/TiO2 (3.2wt. %) doped CMC/PEO.

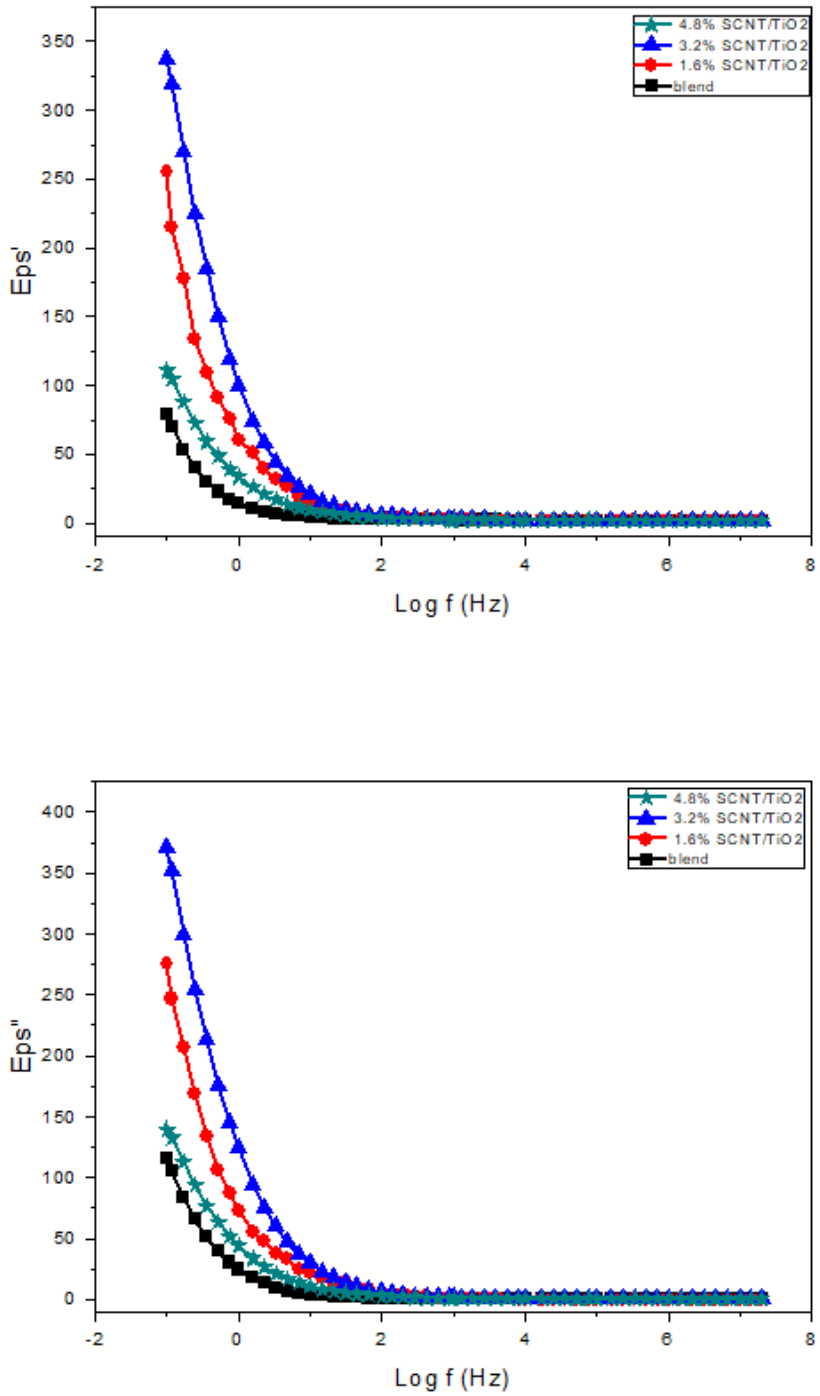

Figure 11

Variation of (a) real ε' and (b) imaginary ε" with f of CMC/PEO and CMC/PEO-(SCNTs/TiO2 wt.%) nanocomposite samples

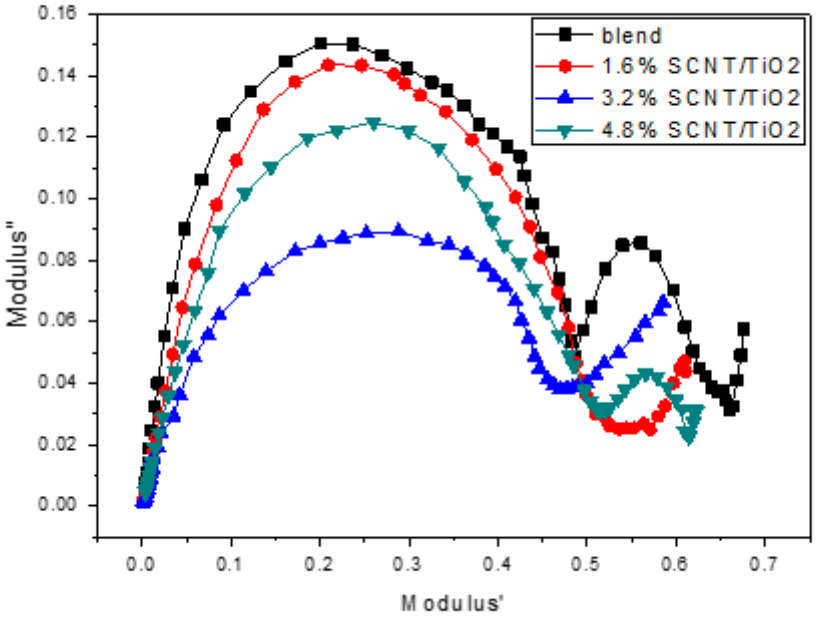

Figure 12

Frequency dependent Cole-Cole plot for of CMC/PEO and CMC/PEO-(SCNTs/TiO2 wt.%) nanocomposite samples

Supplementary Files

This is a list of supplementary files associated with this preprint. Click to download.

- Scheme01.png